

Fast TILs estimation in lung cancer WSIs based on semi-stochastic patch sampling

Nikita Shvetsov^{1*}, Anders Sildnes¹, Lill-Tove Rasmussen Busund^{2,4}, Stig Dalen^{4,5}, Kajsa Møllersen³, Lars Ailo Bongo¹, Thomas K. Kilvaer^{5,6}.

1 Department of Computer Science, UiT The Arctic University of Norway.

2 Department of Medical Biology, UiT The Arctic University of Norway.

3 Department of Community Medicine, UiT The Arctic University of Norway.

4 Department of Clinical Pathology, University Hospital of North Norway.

5 Department of Oncology, University Hospital of North Norway.

6 Department of Clinical Medicine, UiT The Arctic University of Norway.

* Corresponding author: nikita.shvetsov@uit.no

Abstract

Background: The prognostic relevance of tumor-infiltrating lymphocytes (TILs) in non-small cell lung cancer (NSCLC) is well-established. However, manual TIL quantification in whole slide images (WSIs) is laborious and prone to variability. Computational pathology can accelerate and standardize TIL evaluation, resulting in enhanced prognostication and treatment personalization.

Methods: We developed an end-to-end automated pipeline for TIL estimation in lung cancer WSIs, by integrating a semi-stochastic patch sampling approach with a machine learning-based patch classification and cell quantification using HoVer-Net model architecture. The pipeline's performance is evaluated through its computational efficiency, and correlation with patient survival data.

Results: Our pipeline demonstrates the ability to selectively process informative patches, achieving a balance between computational efficiency and prognostic integrity. The patch sampling excluded ~70% of non-informative patches. Further, a selection of only 5% of eligible patches after patch sampling was necessary for cell quantification to retain its prognostic accuracy (c-index 0.65 ± 0.01) resulting in substantial time savings. The pipeline's TILs score correlates strongly with patient survival, outperforming traditional CD8 IHC scoring (c-index 0.59). Kaplan-Meier analysis further substantiated the TILs score's prognostic value.

Conclusion: This study introduces an automated pipeline for TIL evaluation in lung cancer WSIs, providing a prognostic tool with potential to improve personalized treatment in NSCLC. The pipeline's computational advances and clinical relevance demonstrate a step forward in computational pathology, warranting further validation and exploration of its utility in clinical practice.

1. Introduction

Computational pathology is an emerging field set to revolutionize cancer detection and prognostication through faster and more accurate diagnoses and prognoses. Alongside DNA, RNA, radiomics and proteomics, computational pathology is making significant contributions to personalized cancer treatment and has the potential for novel biomarker discovery in clinical settings by shifting from traditional, manual microscope analyses to advanced digital techniques that leverage machine learning and big data [1], [2].

Tumor-infiltrating lymphocytes (TILs) are significant prognostic and potentially predictive biomarkers in numerous cancers [3], [4], [5]. Unfortunately, manual TIL quantification in whole slide images (WSIs) is labor-intensive, subject to bias, and prone to inaccuracies. Hence, TIL quantification is one of the processes where computational pathology may impact clinical implementation leading to improved prognostication for cancer patients.

To reduce the workload of pathologists, a common approach is to estimate the impact of TILs by their total number on a coarse scale or by subjective morphological descriptions [6], [7]. However, even these simple approaches can be time-consuming and may not accurately represent the true condition of the disease. Moreover, although possible, performing detailed computations across all regions of a WSI is impractical due to the immense data volume and may also lead to a degradation in the assessment's performance.

To address these challenges, we present an automated pipeline for efficient TIL evaluation in WSIs. Recognizing that not all areas within a WSI hold equal prognostic value, our pipeline employs a semi-stochastic patch sampling strategy. This approach selectively targets areas with high cell content, samples a fraction of those areas and filters them using only prognostically relevant patches, avoiding the exhaustive analysis of entire slides. By focusing our computational efforts on selected patches, we significantly reduce the time and computational costs, which is crucial for practical applications in clinical and research settings. Our method ensures that the analysis remains viable and scalable, while maintaining the integrity and accuracy of the prognostic evaluation.

This work builds on our previous research, which introduced a pragmatic machine learning methodology for quantifying TILs in tissue from non-small cell lung cancer (NSCLC) patients [8]. Our initial results suggested that our method's prognostic impact could be comparable or even superior to the current standard CD8 immunohistochemical (IHC) staining methods for TIL evaluation in NSCLC. However, our latter effort relied heavily on manual selection of relevant patches to test our model, thus abrogating many of the potential benefits of computational pathology. Herein, we refine this approach by developing an end-to-end pipeline including an automated patch sampling algorithm and patch classification model for identifying prognostically relevant patches.

Our contribution is an efficient and robust automated pipeline for evaluating TILs in WSIs from NSCLC patients. The pipeline presented here enhances the accuracy and reliability of our TILs score by mitigating potential human error and bias. Furthermore, it generates detailed visualizations that highlight areas with high TIL density, offering pathologists insightful information to pinpoint areas of interest and make more informed decisions. In conclusion, our contribution is an automated end-to-end method for TIL evaluation in WSIs that can improve personalized NSCLC treatment.

2. Methods

2.1 Datasets

2.1.1 WSI dataset

The primary dataset comprises complete clinical information and tissue from 553 NSCLC patients treated at the University Hospital of North Norway and Nordland Central Hospital from 1990 to 2010. This cohort has previously been extensively documented [9]. Of these 553 patients, 497 had available WSIs, with each patient having only one WSI accessible for TILs analysis. The process to obtain the results of IHC scores for the different immune cell subsets is described in Kilvaer et al. 2020 [10]. Briefly, tissue-micro arrays comprising two to four tissue cores for each patient in the cohort were stained with IHC to visualize different immune cell subsets, processed in QuPath v.0.1.3 [11]. Thus, a count for each patient was derived based on the mean output of QuPath's built-in positive cell detection algorithm.

The WSIs were captured using an Aperio scanner at x40 magnification in *.svs format and are approximately $10^6 \times 10^6$ pixels at highest resolution. Moreover, these WSIs come with slide-level annotations of viable tumor areas, performed by an experienced pathologist as part of the doMore! project [12]. The annotations, stored as polygons in .xml files, outline the viable tumor areas within each WSI. While the annotations were not directly used in this project, they served as a valuable reference for understanding the overall tumor landscape within the WSIs.

It is important to note that we do not possess a 'ground truth' in terms of labeled cells or reference of TIL density per patch or WSI. Ascertaining a ground truth would require the labeling of millions of cell instances across the 494 WSIs, which is not practically feasible. Therefore, clinical data serves as our reference point for comparison and validation without a precise ground truth.

2.1.2 Patch dataset

Our secondary dataset is an assembly of randomly selected patches from a subset of 194 WSIs derived from the previously mentioned WSI dataset, coupled with lung cancer tiles from the LC25000 dataset [13]. Each patch measures 768 x 768 pixels. The labeled part of dataset was created by an oncologist (TKK) in collaboration with an experienced pathologist (SD) using QuPath [11] and a custom-developed patch annotation tool [14], specifically designed for this project. The process of patch selection and labeling was designed to mitigate potential selection and labeling bias. The labeled data comprises 1628 necrosis, 1913 stroma, 1962 normal lung, and 1069 tumor tissue patches.

To augment the labeled dataset, additional patches were incorporated from the LC25000 dataset. This expansion included 5000 patches each of lung adenocarcinoma, lung squamous cell carcinoma, and benign lung tissue. We integrate the lung adenocarcinoma and lung squamous cell carcinoma patches into tumor tissue class, and the benign lung tissue patches into normal lung class, ensuring a robust and varied dataset for analysis. The combined dataset was then stratified into training and testing sets to train and evaluate patch classification model, described in 2.2.2 section. Specifically, the training set consists of 1350 patches per class, with the remaining patches allocated to the testing set. Consequently, we utilize 74 out of the 194 WSIs used in labeling procedure for training patches, reserving the remaining patches from 120 WSIs for testing and measuring the final patch classification model performance. Downloadable data and description of the patch dataset is available in the data repository [15].

2.2 Algorithms and models

In our prior research, we introduced a pragmatic machine learning methodology to quantify TILs in WSIs from NSCLC patients. We leveraged state-of-the-art deep learning pipeline and training data for cell segmentation and classification, enabling us to identify TILs and provide valuable prognostic insights for NSCLC patients [6]. Specifically, we adapted the HoVer-Net model [8] for our study by retraining it with additional data augmentations, fine-tuned the model to quantify TILs and assessed the results using survival information.

Despite these advancements, our initial evaluation encountered a significant limitation - it was reliant on clinicians manually choosing relevant patches. Hence, abrogating the expected labor-saving benefits of computational pathology, while introducing a potential selection bias. To address these limitations, the goal of the current project was to develop an automated pipeline for evaluating TILs abundance in NSCLC WSIs.

To achieve this, we developed a pipeline combining three consecutive steps: Patch Sampling, Patch Classification, and Cell Quantification. A schematic representation of this pipeline is illustrated in Figure 1. These steps are executed fully automated, yielding visual and quantitative measures of TILs in WSIs. This critical information can aid clinicians in evaluating patient's prognoses and thereby enhancing the overall efficacy and precision of NSCLC diagnoses and treatment planning.

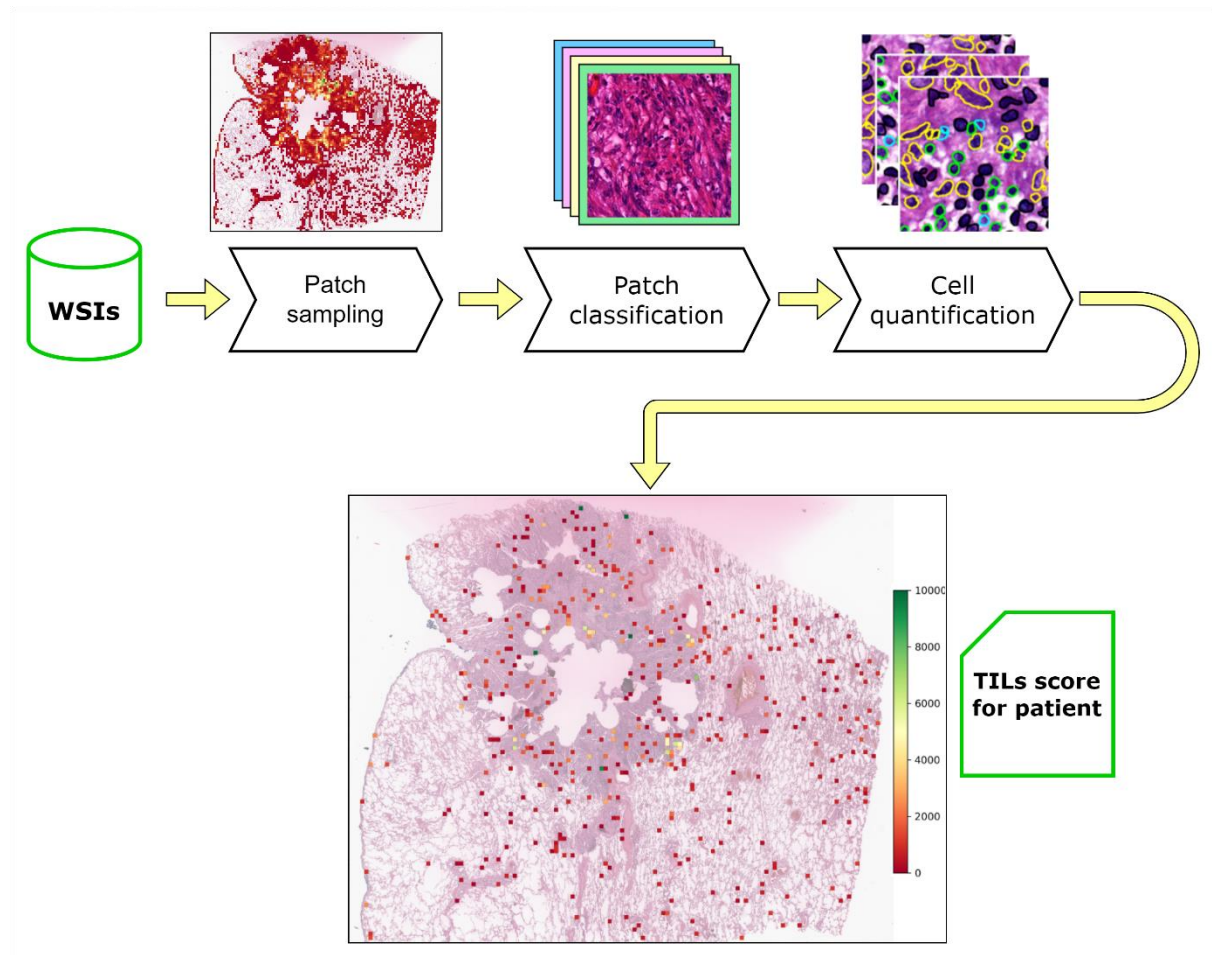


Figure 1. Proposed pipeline for evaluating TILs density in WSI

2.2.1 Patch sampling

In the initial step of the pipeline, we sample patches from WSIs to identify regions with valuable prognostic information. Our semi-stochastic approach targets a fraction of potential patch candidates, hence optimizing the analysis by focusing on meaningful areas. Thus, we avoid exhaustive computations on patches with limited insights.

Tissue extraction: To refine the sampling process, we binarize the image to identify and eliminate non-tissue areas, using the largest contour of any non-empty region as our initial set of patch candidates. Contours are calculated on a downsampled image and then scaled back to the original resolution through an affine transformation. This technique quickly isolates the tissue area without the need for exhaustive analysis.

H-filtering: When a WSI is stained with Hematoxylin and Eosin (H&E), the hematoxylin specifically stains the cell nuclei, while eosin stains other cytoplasmic components and the extracellular matrix. The intensity of the hematoxylin staining correlates with the number of cell nuclei in each area, which in turn reflects the cellular content of that tissue patch. By performing color deconvolution and transforming the RGB image to Hematoxylin-Eosin-DAB (HED) color space [16], we assess the hematoxylin component within each patch. We then compare the mean hematoxylin channel value against a predetermined threshold of 0.017. The threshold is an empirical value derived by visually inspecting a random subset of patches and evaluating respective hematoxylin component maps.

This allows us to effectively filter out empty regions and areas with low cell counts, while preserving patches with sufficient cellular content. Picking a fraction of eligible candidates results in faster execution since subsequent pipeline steps are computationally intensive.

The outcome of this refined sampling is a table of coordinate pairs representing the selected patches. By storing only the coordinates, we conserve computational time and disk space, with a negligible impact on the performance of subsequent algorithmic steps.

This approach balances accuracy and speed, making it a practical solution for high-throughput analysis of WSIs.

2.2.2 Patch classification

The second step in the pipeline is patch classification. The initial filtering leaves some irrelevant patches. In NSCLC diagnostics, pathologists routinely ignore necrotic regions and normal lung tissue due to the minimal prognostic information they offer. By training a model that identifies and excludes necrotic regions and normal lung tissue, we improve the quality and reduce the number of patches included in the final TILs analysis.

We developed a classification model comprising an EfficientNetV2 [17] backbone architecture (V2-S configuration) and a classification head with a dropout layer. The architecture's advanced use of Fused-MBConv blocks and a progressive learning strategy enables it to efficiently handle complex patterns and emphasize prominent features within the detailed tissue images. EfficientNetV2's improved scaling method and training speed optimizations align with the demands of histopathology, scaling up the network to process large images, ensuring detailed pattern recognition in tissue structures, while being parameter efficient and computationally less demanding during training.

For training and testing the patch classifier model, we utilize the patch dataset described in 2.1.2 section. In the model training phase, we implemented a 5-fold cross-validation strategy utilizing our designated training dataset to ensure robustness and generalizability of our model. To mitigate the

risk of overfitting, a series of augmentation techniques were employed. These techniques included affine transformations, such as translation, scaling, and rotation, to simulate variability in tissue sample positioning. Moreover, we randomly enhanced tissue contrast and modified stain concentration to account for variations in histological processing. Additionally, we applied random normalization based on the Macenko algorithm [18], [19] to standardize the staining appearance across different samples.

The output of this step is a modified table from the patch sampling step, with a class label assigned to each patch. Patch filtering facilitates the identification of relevant patches for further analysis.

2.2.3 Cell quantification

The third step in the pipeline is cell quantification. During this step, we process the list of patches, selecting those that correspond to the 'tumor tissue' and 'stroma' classes within the patch dataset, which include tumor tissue, stroma, tertiary lymphoid structures, and areas with TILs. For each selected patch, we extract its coordinates, retrieve the patch from the corresponding WSI, apply the necessary preprocessing, and perform inference using a modified version of HoVer-Net based model trained on the PanNuke dataset [20]. The choice of the PanNuke dataset was based on its diversity and the substantial amount of labeled cell nuclei. The trained model delineates cellular structures, classifies them, and quantifies TILs. This quantification pipeline has been adapted from our earlier study [8].

Upon quantifying the cells, we obtain raw TIL counts within each patch. To enable comparison across different patches and WSIs, we normalize these counts by the area of the patch, accounting for the resolution of the WSI. The normalization formula (1), adjusted for square micrometers and standardized to cells per square millimeter, is as follows:

$$d_i = \frac{c_i}{(\text{patch_size} \times \text{mpp})^2} \times 10^6 \quad (1)$$

Here, d_i represents the density of TILs in cells per square millimeter for patch i , c_i is the absolute TIL count for patch i , patch_size is the width or height of the patch in pixels, and mpp is the microns-per-pixel ratio of the WSI. The factor 10^6 is applied to convert the area from square microns to square millimeters.

For a given patient, the final TIL density score, d_{patient} , is computed as the mean density across all patches within the WSI. In our current cohort, each patient is represented by a single WSI, hence, the calculation of d_{patient} (2) does not require averaging across multiple slides:

$$d_{\text{patient}} = \frac{1}{n} \sum_{i=1}^n d_i \quad (2)$$

It is important to note that for studies with multiple WSIs per patient, the final TIL density score would be the average density across all patches and all k WSIs for the patient, as represented by the formula (3):

$$d_{\text{patient}} = \frac{1}{k} \sum_{j=1}^k \left(\frac{1}{n_j} \sum_{i=1}^{n_j} d_i \right) \quad (3)$$

However, this additional averaging step is not required in the context of our investigated cohort.

2.3 Results visualization

The results can be visualized by assigning a TILs score for each patch and constructing a heatmap as visualized in Figure 2. In this WSI, the TILs score varies from 0 (no TILs) to ≥ 10000 (extremely high, TILs density clipped at 10000 to due to outliers). This visualization provides a comprehensive overview of TILs distribution across the WSI, further enhancing pathologists' vision and understanding of the tumor microenvironment and its potential implications on patient prognosis.

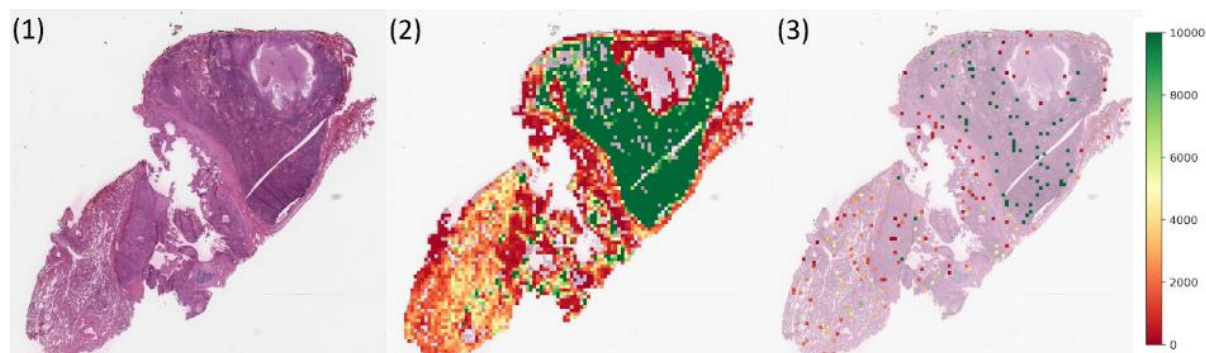


Figure 2. Example of TILs score visualization. (1) Original WSI, (2) all patch candidates, (3) 5% of patch candidates

2.4 Pipeline implementation

We implement our pipeline in Python v3.10 [21] and PyTorch v2.1.0 [22]. To efficiently access and manipulate data from WSIs, we utilized the OpenSlide v4.0.0 [23], libvips v8.15.0 [24], opencv v4.9.0 [25] and scikit-image v0.22.0 [26] libraries. The pipeline has a modular structure and can be parallelized at the WSI level, and even within steps. For instance, patch sampling can be distributed across a pool of processes, and the patch classification and cell quantification steps can utilize multiple GPUs to accelerate processing. However, for comparison and debugging purposes, parallel processing was not involved in validation runs. The development and validation were performed on a machine with an Intel Xeon W-2255 CPU with 10 cores and an RTX Titan GPU with 24 GB VRAM. The source code of the pipeline and trained models are available on GitHub [27].

2.5 Data analysis

To investigate the prognostic potential of TILs in NSCLC, we perform statistical analysis to highlight relationship between TILs, clinicopathological characteristics and their combined impact on patient outcomes. The goal is to identify if TILs score can serve as a reliable indicator of patient survival and how it compares to the current standard IHC staining approach.

Correlations between our TILs score, clinicopathological variables and dichotomized cell counts for different immune cell subsets were calculated using the χ^2 or Fishers exact test whenever appropriate. Disease-specific survival, defined as the time from diagnosis to lung cancer related death, was the chosen endpoint for survival analyses. Survival curves were calculated using the Kaplan Meier method and the difference between groups was tested using the log-rank test. The prognostic performance of obtained TIL score, relative to cell counts for different immune cell subsets, was quantified using the concordance index (c-index), which serves a role analogous to the AUROC by measuring the model's discriminative ability in correctly ranking patients according to survival risk. To assess the prognostic impact of our TILs score in relation to other clinical variables,

multivariable models using the Cox proportional hazards models were created. The significance level used throughout this study was $p < 0.05$. For our analyses we used the Pandas v2.2.0 [28], and lifelines v0.27.8 [29] python libraries and R version 4.3.1 [30] with the survival v3.5-7 [31] library.

3. Results

The following sections provide a comprehensive description of the performance and impact of our pipeline. Briefly summarized we correlate patient level TILs scores to prognosis to demonstrate its potential impact on lung cancer treatment.

3.1 Patch sampling

The patch sampling process was quantitatively assessed by two key metrics: the proportion of patches excluded, and the execution time required for the sampling procedure. Initially, the algorithm filters out approximately 70% of the total patches, which are identified as non-informative due to their absence of tissue or insufficient cellular content. This preliminary reduction is executed with an average processing time of 5 minutes per WSI, corresponding to a throughput of 20 patches per second on a single-threaded process. Figure 3 illustrates a representative example of eligible patch sampling candidates for a 768 x 768 size.

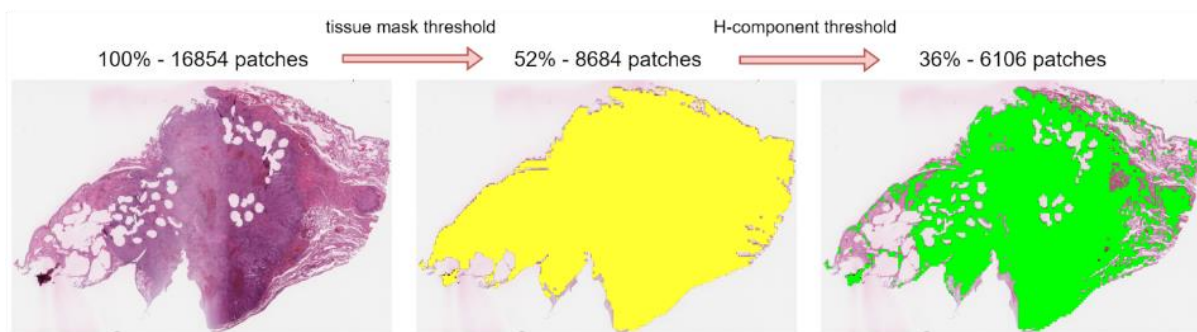


Figure 3. Patch sampling reduction process with tissue mask and H-component thresholding

After initial exclusion, we employ a random sampling strategy, where we select 5% of the remaining eligible patches for tissue classification and TILs quantification analysis. This two-step process was designed to achieve a balance between computational complexity and the preservation of critical prognostic information contained in the slide. The selection of a 5% sampling ratio was determined through an empirical evaluation of 50 WSIs. We systematically decreased the number of candidate patches utilized in the calculation of the concordance index using Monte-Carlo simulation. This iterative reduction continued until we achieved a balance between a stable concordance score and a computationally efficient time ratio, ensuring both representativeness of the sampled patches and optimal performance of the pipeline. The analyzed range from 50% to 0.5% is shown in Appendix Table A2.1. By implementing this two-step sampling approach, we concentrated subsequent computations on a mere 2% of the total patches per WSI. This reduction speeds up the analysis significantly while still maintaining the high-level prognostic information needed for treatment decision-making.

3.2 Patch classification

The patch classification step aims to further reduce the subset of patches by excluding prognostically irrelevant regions. This step's performance was evaluated by its classification accuracy and impact on execution time for the subsequent pipeline stage.

The accuracy of the patch classification process was assessed by comparing the predicted class labels with the ground truth labels in the test subset of our patch dataset. The test subset was clipped to the number of patches of the least represented class, leaving 295 patches of each class for testing. Our EfficientNetV2-based patch classifier model was trained using 5-fold cross-validation, with ensured class balance within each fold. The model achieved an aggregated accuracy of 86.44% and multiclass Area Under the Receiver Operating Characteristic (average of the one-vs-rest AUCs) of 97.36%, demonstrating its effectiveness in distinguishing between patches with high density of necrotic cells or normal lung tissue and patches with tumor tissue and stroma. A comprehensive overview of the model's performance on the test subset is provided by the confusion matrix (Appendix Figure A2.1).

The patch classification process demonstrates its efficiency by quickly processing and classifying patches. On average, the patch classification model classified 1000 patches in 60 seconds using GPU, highlighting its potential for rapid analysis of lung cancer tissue.

The impact of the patch classification process on the pipeline's subsequent stages was significant. By assigning a class label to each patch and filtering out irrelevant patches, we were able to reduce the number of quantified patches, while preserving the possibility to visually inspecting patches that were included and discarded for the subsequent cell quantification step. On average, 15% of the patches (necrotic and normal lung tissue) were discarded during this step. Figure 4 illustrates the patch classification step, showing examples of the patch classes found in the slide on the left and eligible patches on the right.

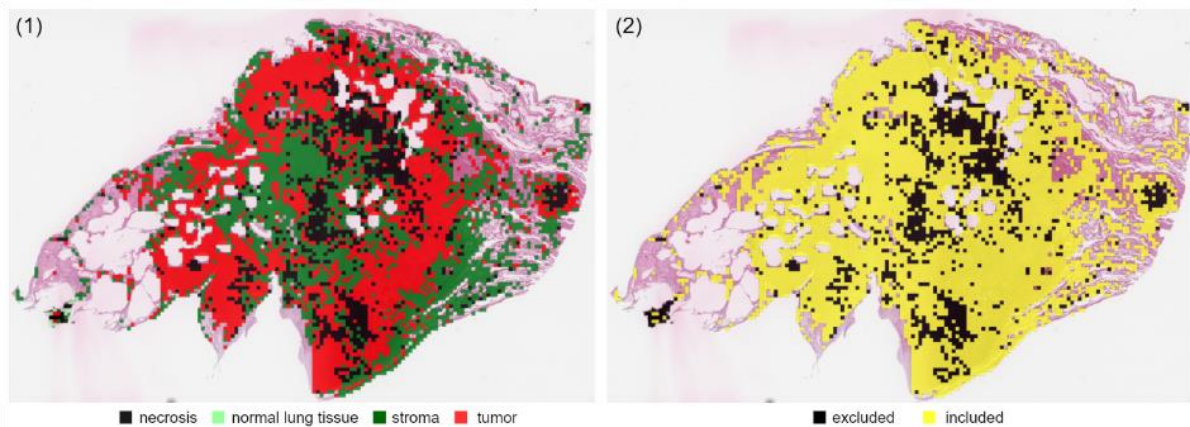


Figure 4. Patch classification step visualization: (1) Color coded patch classification, (2) Patch selection, based on classes

3.3 Cell quantification

The final stage of our pipeline involves cell quantification, focusing on TILs. While the generation of explanatory masks for segmented cellular instances is an optional feature, the process remains computationally intensive, due to the three separate decoding branches of the modified HoVer-Net architecture, along with the detailed post-processing of the resulting pixel maps. Our pipeline has

been designed to automatically decrease the number of patches requiring analysis, so this reduction helps to mitigate the intensive computational demands of this stage.

We utilize a modified version of the HoVer-Net model, trained on the PanNuke dataset for this purpose. The model performance is well described in Shvetsov et al. 2022 [8]. We evaluate the model's performance using Dice score (DICE), achieving 82.48%, Jaccard score (or also known as intersection over union (IoU)) of 90.87%, and panoptic quality score (PQ) of 52.07% on our test subset. These metrics, defined in Appendix A1.1, confirm the model's capability in delineating and classifying cellular structures.

By normalizing the absolute TIL counts and calculating the cell density for each patch, we were able to obtain a comprehensive TILs score for each WSI. This score can be used for further analysis and prognosis. To illustrate how the score reflects TILs density within the patch, we visualize and evaluate TILs score for patches in WSIs. Figure 5 shows a patch with just a few TILs, a patch with mean density of TILs and the patch with maximum TILs score from a single WSI. The score can represent TILs density, given patch size, raw TILs counts and slide resolution.

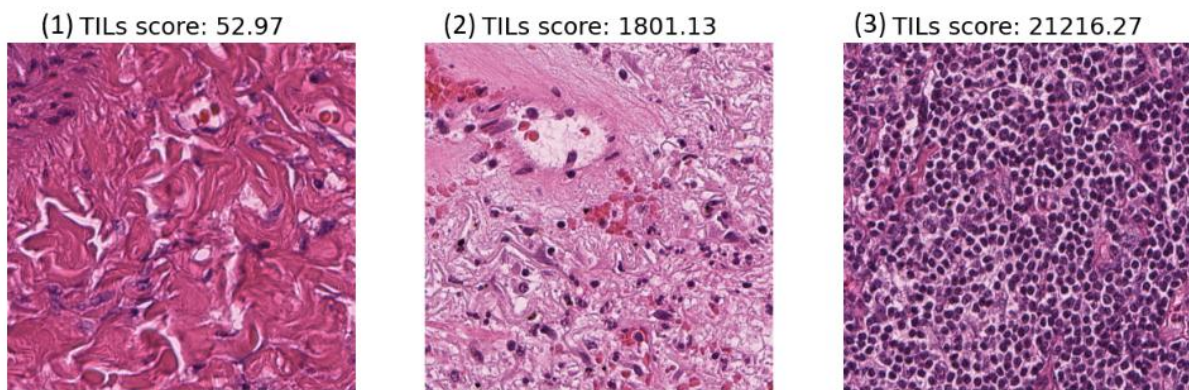


Figure 5. Example of TILs score for 768x768 patches (1) with small amount of TILs, (2) mean amount across slide and (3) maximum amount across slide

3.4 Optimization and time analysis

To evaluate pipeline performance in terms of computational efficiency we conducted a time analysis using a subset of 50 WSIs. For each WSI, the number of patches varies in accordance with factors such as WSI size, the presence of artifacts, and the extent of necrotic areas. To account for these variations, we present an average time for each pipeline step, as recorded across the analyzed WSIs.

The data in Table 1 shows a degree of reduction in processing time when analyzing only 5% of the patches compared to the full set. Evaluations showed that processing time increases linearly as we increase patch ratio. Specifically, when considering the entire patch cohort (100%), the average patch sampling, classification, and quantification times are 5.4, 4.7, and 72.5 minutes, respectively. Conversely, when the analysis is confined to 5% of the patches, these times are reduced to 18 seconds for sampling, 15 seconds for classification, and 3.6 minutes for quantification.

The optimization was achieved through the targeted analysis of a 5% patch subset. This not only conserves computational resources but also significantly accelerates the pipeline, a critical factor for clinical applicability where expedient results may influence treatment decisions.

Moreover, it is critical to underscore that the decision to analyze a reduced subset of patches does not stem solely from a desire to improve processing time. Our empirical evidence (Appendix Table A2.1) suggests that utilizing the full collection of patches does not confer additional prognostic value,

while having a small fraction of analyzed patches provides good prognostic, as we show in subsequent section.

Analyzed Patch Ratio	Patch Sampling time (average)	Patch Classification time (average)	Patch Quantification time (average)
100%	5 minutes 23 sec	4 minutes 44 sec	72 minutes 32 sec
70 %	3 minutes 47 sec	3 minutes 22 sec	50 minutes 45 sec
50 %	2 minutes 42 sec	2 minutes 24 sec	36 minutes 15 sec
20 %	1 minute 5 sec	57 seconds	14 minutes 30 sec
5%	18 seconds	15 seconds	3 minutes 37 sec

Table 1. Average performance of pipeline steps at different patch analysis ratios

Therefore, the efficiency gained in analysis time does not come at the cost of prognostic accuracy.

3.5 Clinical validation and statistical analysis

To evaluate the overall clinical value of the pipeline, we utilized clinical data for 429 WSIs in our patient cohort, that did not contribute to patch classifier training and tuning. For subgroup analyses in LUSC (lung squamous cell carcinoma) and LUAD (lung adenocarcinoma) histologies and in pathological stages (pStage), we used the full dataset to retain statistical power.

Unfortunately, given our pipeline's multi-stage nature, it is challenging to isolate and measure each stage's impact separately. However, the pipeline's overall performance can be obtained by estimating the prognostic impact of the final TILs score. For ease of interpretation in survival analyses and for comparison with clinicopathological variables, we quantize the TILs score into four groups based on quantile cut-offs obtained from overall cohort.

Our evaluations of the TILs score as a prognostic factor are presented in Table 2. A high TILs score was associated with a favorable prognosis in both uni- and multivariable analyses of the overall cohort and subgroups according to histology and pStage. This pattern across different patient groups suggests that the TILs score is a viable indicator of a patient's prognosis. The data indicates that patients with a higher abundance of TILs tend to have a better overall prognosis. In our cohort, those in the uppermost quartile of TILs scores (Q4) were found to have a significantly lower risk when compared to those in the lowest quartile (Q1). This inverse relationship between TILs scores and risk highlights the score's role in stratifying patients based on their immune response to the tumor.

To further investigate the prognostic value of the TILs score, we conducted a comparison with the CD8 IHC score for disease-specific survival in non-small cell lung cancer patients, as detailed in Appendix Table A3.3. The analysis indicates that the TILs score has a more consistent association with improved 5-year survival rates and median survival times across the overall, validation, and training cohorts.

Kaplan-Meier survival analysis provides visual support for our findings, with a notable difference between the prognostic markers. The Kaplan-Meier curves for CD8 IHC score (Figure 6) display a significant degree of overlap among the various risk groups, which could imply a limitation in their prognostic utility. In contrast, the Kaplan-Meier curves for the TILs score (Figure 7) demonstrate a more pronounced separation between risk levels. This separation is especially prominent when comparing the highest and lowest TILs score quartiles, suggesting that the TILs score offers better prognostic value.

	Overall cohort		Validation cohort		Overall cohort		Overall Cohort	
	All patients		All patients		LUSC subset		LUAD subset	
	HR(95% CI)	<i>p</i>	HR(95% CI)	<i>p</i>	HR(95% CI)	<i>p</i>	HR(95% CI)	<i>p</i>
ECOG								
0	1.		1.		1.			
1	1.32(0.95-1.84)	0.097	1.32(0.95-1.84)	0.097				
2	1.14(0.55-2.36)	0.726	1.14(0.55-2.36)	0.726				
Differentiation								
Poor	1.		1.				1.	
Moderate	0.83(0.59-1.16)	0.268	0.83(0.59-1.16)	0.268			0.94(0.61-1.46)	0.794
Well	0.4(0.23-0.72)	0.002	0.4(0.23-0.72)	0.002			0.38(0.2-0.72)	0.003
pStage								
I	1.		1.		1.		1.	
II	1.49(0.99-2.23)	0.054	1.49(0.99-2.23)	0.054	1.51(0.88-2.59)	0.130	1.57(0.95-2.61)	0.078
III	3.69(2.51-5.42)	<0.001	3.69(2.51-5.42)	0.000	4.68(2.76-7.91)	<0.001	3.47(2.11-5.72)	<0.001
TILs score								
Q1	1.		1.		1.		1.	
Q2	0.74(0.5-1.08)	0.120	0.74(0.5-1.08)	0.120	1.01(0.61-1.66)	0.981	0.46(0.27-0.78)	0.004
Q3	0.51(0.33-0.78)	0.002	0.51(0.33-0.78)	0.002	0.47(0.24-0.92)	0.027	0.41(0.24-0.71)	0.001
Q4	0.3(0.19-0.49)	<0.001	0.3(0.19-0.49)	<0.001	0.29(0.15-0.53)	<0.001	0.32(0.17-0.6)	<0.001

Table 2. Hazard ratios for clinical and pathological prognostic factors in validation cohort and in the LUSC and LUAD subgroups

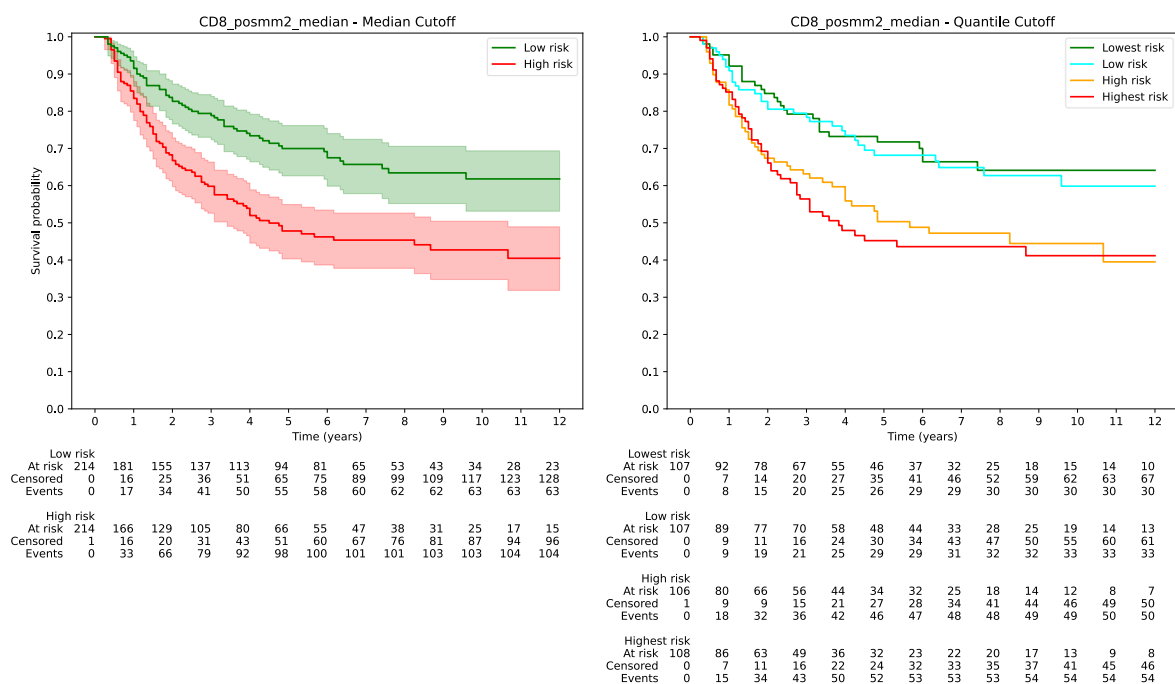


Figure 6. Kaplan-Meier curves for CD8 IHC score

We also evaluate the statistical associations between the TILs score and clinicopathological variables in Appendix Table A3.1 and between the TILs score and IHC based markers of common immune cells markers in Appendix Table A3.2. The TILs score was significantly associated with LUSC (Lung

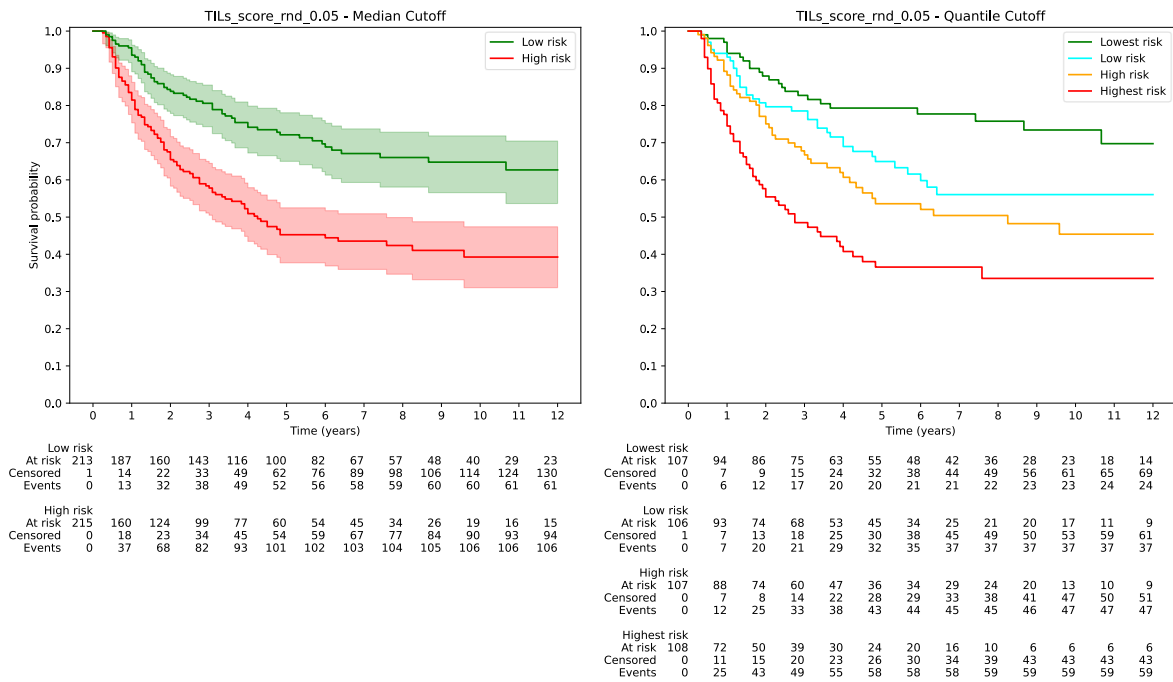


Figure 7. Kaplan–Meier curves for TILs score

squamous cell carcinoma) histology and immune cell expression of CD3 (pan T-cells), CD4 (helper T-cells), CD8 (cytotoxic T-cells) and CD20 (B-cells).

Lastly, we compare the overall prognostic ability of the TILs score to that of the CD8 immunohistochemistry (IHC) score, using the c-index. The c-index helps us understand how well a certain factor can help predict outcomes in a survival model. In our case, we are looking at the TILs score and the CD8 IHC score. The c-index goes from 0.5 (no prognostic value) to 1.0 (perfect at predicting outcomes). The TILs score for 5% of patch candidates got a c-index of 0.649, while the CD8 score got a c-index of 0.599.

To validate the chosen ratio, of 5% we conducted a series of experiments on a subset of 50 WSIs, assigning unique seed values to each to guarantee a diverse selection of patches. Our findings (Appendix Table A2.1) indicated that within the 0.5% to 50% sampling range, there was no significant impact on the final model's prognostic accuracy (c-index 0.65 ± 0.01). This evidence supports the efficacy of the 5% threshold in our cohort, confirming that it conserves computational resources without detracting from the model's diagnostic performance.

4. Discussion

In this study, we have developed an automated, fast, and low-resource usage pipeline for the rapid analysis of high cell density patches, that possess prognostic information, from WSIs of lung cancer tissue. The pipeline integrates computer vision techniques for efficient patch sampling and state-of-the-art deep learning models for classification and cell quantification. It represents a valid contribution in computational pathology and in NSCLC prognostication as the pipeline prognostic performance compares favorably to other approaches for TIL evaluation in NSCLC.

Our results demonstrate the pipeline's ability to select informative patches from WSIs, quantify cells and produce TILs density approximation for WSI, with patch-level TILs density visualizations for

further investigation by pathologist. The patch sampling process rapidly delineated the tissue area and identified patches with a high enough cell count. The patch classification process achieved high accuracy in distinguishing between patches with high density of necrosis and/or normal lung tissue and patches with tumor tissue and/or tumor associated stroma. The cell quantification process was effective in delineating cellular structures and classifying them, as demonstrated by the high scores achieved by our model.

In our study, we conducted an ablation experiment to assess the impact of the patch classification step on the pipeline's performance. This comparison revealed that the inclusion of a patch filtering process enhanced the c-index by 0.05. This increment indicates that patch filtering plays a role in isolating patches with high prognostic value, thereby underlining its significance in the pipeline's overall accuracy.

A pivotal aspect of our pipeline's design is the determination of the optimal ratio of patches to be analyzed for robust TILs evaluation. Through extensive experimentation, we have established that the pipeline's performance remains stable across a spectrum of analyzed patches, ranging from 1% to 50% of the filtered candidates. This stability is indicative of the robustness of our TILs scoring algorithm and its insensitivity to the volume of data processed by the latter pipeline stage. Crucially, our analyses indicate that an optimal threshold exists at approximately 5% of patch candidates, averaging around 350 patches per WSI for our cohort. At this level, we observed a c-index of around 0.65 with a minimal standard deviation of 0.002, presenting a compelling case for testing of this ratio for other data sources for validation. This 5% threshold represents a sensible trade-off between computational load and prognostic accuracy.

The modular structure of our pipeline allows for potential parallelization at the WSI level and even within steps, which could further enhance its execution time. Moreover, the pipeline's ability to provide explanations in the form of masks and patch label overlays could be adapted to assist pathologists in identifying suspicious cases and potentially improve the accuracy of lung cancer prognosis. Our proposed patch sampling and classification procedures significantly reduce the number of patches requiring quantification, which traditionally could extend to several hours per slide and yield less accurate WSI level TILs scores. In terms of prognostic impact, the TILs score, generated by our pipeline, demonstrated a higher prognostic accuracy compared to the current CD8 IHC score. This underlines the dual advantage of our pipeline: improved computational efficiency and accuracy of TILs evaluation in WSI.

While our study presents promising results, there are some limitations. The multi-stage nature of our pipeline, where each subsequent step is dependent on the results of the previous one, poses a challenge in measuring the impact of each stage separately due to the absence of ground truth labels for each stage. This limitation hinders our ability to quantitatively assess the individual contribution and performance of each stage.

Furthermore, despite our patch sampling filtering techniques, some patches with low prognostic information may still be included. The opposite scenario is also possible, as the patch classifier may misclassify necrotic or normal lung regions. This was evident in the confusion matrix (Figure A2.1), which indicated a higher rate of misclassifications for the 'necrosis' class compared to others. Such misclassifications could lead to an underestimation of necrotic regions, subsequently influencing the TILs density score.

Future work could also focus on refining the patch sampling process to further reduce the number of irrelevant patches, extracting patches from relevant regions, e.g. tumor border, where abundance of

TILs may be indicative of a stronger immune response to the tumor growth and include other cell types that are known for their prognostic or even predictive properties in NSCLC [32].

For a more complete representation of the pipeline's performance, future iterations of this study could include a more detailed breakdown of the computational cost analysis, accounting for electricity usage, could provide a full view of our approach's cost-effectiveness. Furthermore, comparing the performance of the pipeline on a heterogeneous set of hardware configurations would be beneficial to understand its scalability and to identify potential bottlenecks in diverse clinical settings.

5. Conclusions

In conclusion, this study introduces a novel, automated pipeline for efficient TILs evaluation in WSIs. Our results suggest that the TILs score, generated by our pipeline, offers improved prognostic power compared to the current CD8 IHC score. This is evidenced by the superior c-index and the more distinct separation of high and low risk groups in the Kaplan-Meier survival curves generated by our TILs score. The pipeline also provides explainable heatmaps and patch visualizations across WSIs.

The developed pipeline integrates computer vision techniques and state-of-the-art deep learning models for efficient patch sampling, classification, and cell quantification. Specifically, the pipeline maintains high accuracy, while also demonstrating computational efficiency and speed. This is achieved despite the large volume of patches contained in the WSIs and the complex models required to accurately quantify overlapping cells in these images. The ability to process and evaluate patches on-the-fly, without the need to save them to disk, coupled with an efficient patch sampling algorithm and a reduced number of patches for cell quantification, underscores the pipeline's superior performance to current clinical approach in terms of speed and computational resource utilization, while also being a promising method for TILs quantification and NSCLC prognosis. It could improve current clinical practice through more accurate and personalized treatment strategies for lung cancer patients.

Further studies are needed to validate these findings. The clinical applicability of our pipeline also needs to be assessed in more detail. Future research should focus on these aspects, exploring the full potential of our approach by investigating other biomarkers for improving NSCLC prognosis and transforming the landscape of computational pathology.

References

- [1] D. Cifci, G. P. Veldhuizen, S. Foersch, and J. N. Kather, "AI in computational pathology of cancer: Improving diagnostic workflows and clinical outcomes?," *Annu. Rev. Cancer Biol.*, vol. 7, no. 1, Apr. 2023.
- [2] B. Acs, M. Rantalainen, and J. Hartman, "Artificial intelligence as the next step towards precision pathology," *J. Intern. Med.*, vol. 288, no. 1, pp. 62–81, Jul. 2020.
- [3] M. J. M. Gooden, G. H. de Bock, N. Leffers, T. Daemen, and H. W. Nijman, "The prognostic influence of tumour-infiltrating lymphocytes in cancer: a systematic review with meta-analysis," *Br. J. Cancer*, vol. 105, no. 1, pp. 93–103, Jun. 2011.
- [4] R. Salgado *et al.*, "The evaluation of tumor-infiltrating lymphocytes (TILs) in breast cancer: recommendations by an International TILs Working Group 2014," *Ann. Oncol.*, vol. 26, no. 2, pp. 259–271, Feb. 2015.
- [5] S. Hendry *et al.*, "Assessing Tumor-Infiltrating Lymphocytes in Solid Tumors: A Practical Review for Pathologists and Proposal for a Standardized Method from the International Immunology Biomarkers Working Group: Part 2: TILs in Melanoma, Gastrointestinal Tract Carcinomas, Non-Small Cell Lung Carcinoma and Mesothelioma, Endometrial and Ovarian Carcinomas, Squamous Cell Carcinoma of the Head and Neck, Genitourinary Carcinomas, and Primary Brain Tumors.," *Adv Anat Pathol*, vol. 24, no. 6, pp. 311–335, Nov. 2017, doi: 10.1097/PAP.000000000000161.
- [6] S. Loi *et al.*, "Tumor-Infiltrating Lymphocytes and Prognosis: A Pooled Individual Patient Analysis of Early-Stage Triple-Negative Breast Cancers.," *J Clin Oncol*, vol. 37, no. 7, pp. 559–569, Mar. 2019, doi: 10.1200/JCO.18.01010.
- [7] M. Rakaee *et al.*, "Machine learning-based immune phenotypes correlate with STK11/KEAP1 co-mutations and prognosis in resectable NSCLC: a sub-study of the TNM-I trial," *Annals of Oncology*, vol. 34, no. 7, pp. 578–588, Jul. 2023, doi: 10.1016/j.annonc.2023.04.005.
- [8] N. Shvetsov *et al.*, "A Pragmatic Machine Learning Approach to Quantify Tumor-Infiltrating Lymphocytes in Whole Slide Images.," *Cancers (Basel)*, vol. 14, no. 12, Jun. 2022, doi: 10.3390/cancers14122974.
- [9] S. M. Hald *et al.*, "LAG-3 in Non-Small-cell Lung Cancer: Expression in Primary Tumors and Metastatic Lymph Nodes Is Associated With Improved Survival.," *Clin Lung Cancer*, vol. 19, no. 3, pp. 249–259.e2, May 2018, doi: 10.1016/j.clcc.2017.12.001.
- [10] T. K. Kilvaer *et al.*, "Digitally quantified CD8+ cells: the best candidate marker for an immune cell score in non-small cell lung cancer?," *Carcinogenesis*, vol. 41, no. 12, pp. 1671–1681, Dec. 2020, doi: 10.1093/carcin/bgaa105.
- [11] P. Bankhead *et al.*, "QuPath: Open source software for digital pathology image analysis," *Scientific Reports*, vol. 7, no. 1, p. 16878, 2017, doi: 10.1038/s41598-017-17204-5.
- [12] "DoMore!," Doing more to provide faster and safer cancer prognostics. [Online]. Available: <https://www.domore.no/>
- [13] A. A. Borkowski, M. M. Bui, L. B. Thomas, C. P. Wilson, L. A. DeLand, and S. M. Mastorides, *Lung and Colon Cancer Histopathological Image Dataset (LC25000)*. 2019.
- [14] N. Shvetsov, "Patch labeler." 2023. [Online]. Available: <https://github.com/nik-shvetsov/flet-patch-labeler>
- [15] Shvetsov Nikita, Thomas Karsten Kilvaer, and Stig Manfred Dalen, "UNN-LC High-Resolution Histopathological Lung Tissue Patch Dataset." *DataverseNO*, 2024. doi: 10.18710/ZZASBA.
- [16] A. Ruifrok and D. Johnston, "Ruifrok AC, Johnston DA. Quantification of histochemical staining by color deconvolution. *Anal Quant Cytol Histol* 23: 291-299," *Analytical and quantitative cytology and histology / the International Academy of Cytology [and] American Society of Cytology*, vol. 23, pp. 291–9, Sep. 2001.
- [17] M. Tan and Q. V. Le, *EfficientNetV2: Smaller Models and Faster Training*. 2021.

- [18] M. Macenko *et al.*, "A method for normalizing histology slides for quantitative analysis," in *2009 IEEE International Symposium on Biomedical Imaging: From Nano to Macro*, Jul. 2009, pp. 1107–1110. doi: 10.1109/ISBI.2009.5193250.
- [19] Y. Zhou, *CielAI/torch-staintools: V1.0.3 Release*. Zenodo, 2024. doi: 10.5281/zenodo.10453807.
- [20] J. Gamper *et al.*, "PanNuke Dataset Extension, Insights and Baselines," *arXiv preprint arXiv:2003.10778*, 2020.
- [21] G. Van Rossum and F. L. Drake, *Python 3 Reference Manual*. Scotts Valley, CA: CreateSpace, 2009.
- [22] A. Paszke *et al.*, "PyTorch: An Imperative Style, High-Performance Deep Learning Library," in *Advances in Neural Information Processing Systems 32*, Curran Associates, Inc., 2019, pp. 8024–8035. [Online]. Available: <http://papers.neurips.cc/paper/9015-pytorch-an-imperative-style-high-performance-deep-learning-library.pdf>
- [23] A. Goode, B. Gilbert, J. Harkes, D. Jukic, and M. Satyanarayanan, "OpenSlide: A vendor-neutral software foundation for digital pathology.," *J Pathol Inform*, vol. 4, p. 27, 2013, doi: 10.4103/2153-3539.119005.
- [24] J. Cupitt and K. Martinez, "VIPs: An imaging processing system for large images," *Proceedings of SPIE - The International Society for Optical Engineering*, vol. 1663, Feb. 1996, doi: 10.1117/12.233043.
- [25] G. Bradski, "The OpenCV Library," *Dr. Dobb's Journal of Software Tools*, 2000.
- [26] S. Van der Walt *et al.*, "scikit-image: image processing in Python," *PeerJ*, vol. 2, p. e453, 2014.
- [27] N. Shvetsov, "fastCellScore pipeline." 2024. [Online]. Available: <https://github.com/nik-shvetsov/fastCellScore>
- [28] W. McKinney and others, "Data structures for statistical computing in python," in *Proceedings of the 9th Python in Science Conference*, Austin, TX, 2010, pp. 51–56.
- [29] C. Davidson-Pilon, "lifelines: survival analysis in Python," *Journal of Open Source Software*, vol. 4, no. 40, p. 1317, 2019.
- [30] R Core Team, *R: A Language and Environment for Statistical Computing*. R Foundation for Statistical Computing, 2018. [Online]. Available: <https://www.R-project.org/>
- [31] T. M. Therneau, *A Package for Survival Analysis in R*. 2024. [Online]. Available: <https://CRAN.R-project.org/package=survival>
- [32] M. Rakaee *et al.*, "Prognostic Value of Macrophage Phenotypes in Resectable Non–Small Cell Lung Cancer Assessed by Multiplex Immunohistochemistry," *Neoplasia*, vol. 21, no. 3, pp. 282–293, Mar. 2019, doi: 10.1016/j.neo.2019.01.005.

Acknowledgments

This work was supported by the High North Population Studies, UiT The Arctic University of Norway. This work was funded in part by the Research Council of Norway grant no. 309439 SFI Visual Intelligence, and the North Norwegian Health Authority grant no. HNF1521-20.

Appendix

A1. Supplementary Methods

A1.1 Definition of metrics used to evaluate the performance of the cell segmentation model

The results of our cell segmentation pipeline are detailed in Shvetsov et al 2022. Briefly, we used the following definitions of metrics to evaluate the cell segmentation pipeline:

- 1) $DICE = \frac{2*TP}{2*TP+FP+FN}$, where TP and FP represent the number of true positive and false positive pixels, respectively.
- 2) $IoU = \frac{\sum_{i=1}^n |X_i \cap Y_i|}{\sum_{i=1}^n |X_i \cup Y_i|}$, where n represents the number of classes, where X_i represents the set of pixels predicted to belong to class i, and Y_i represents the set of pixels that belong to class i in the ground truth.
- 3) $PQ = \frac{IOU}{TP+0.5FP+0.5FN}$, where TP, FP and FN represent the number of true positives, false positive and false negative pixels, respectively.

A2. Supplementary Results

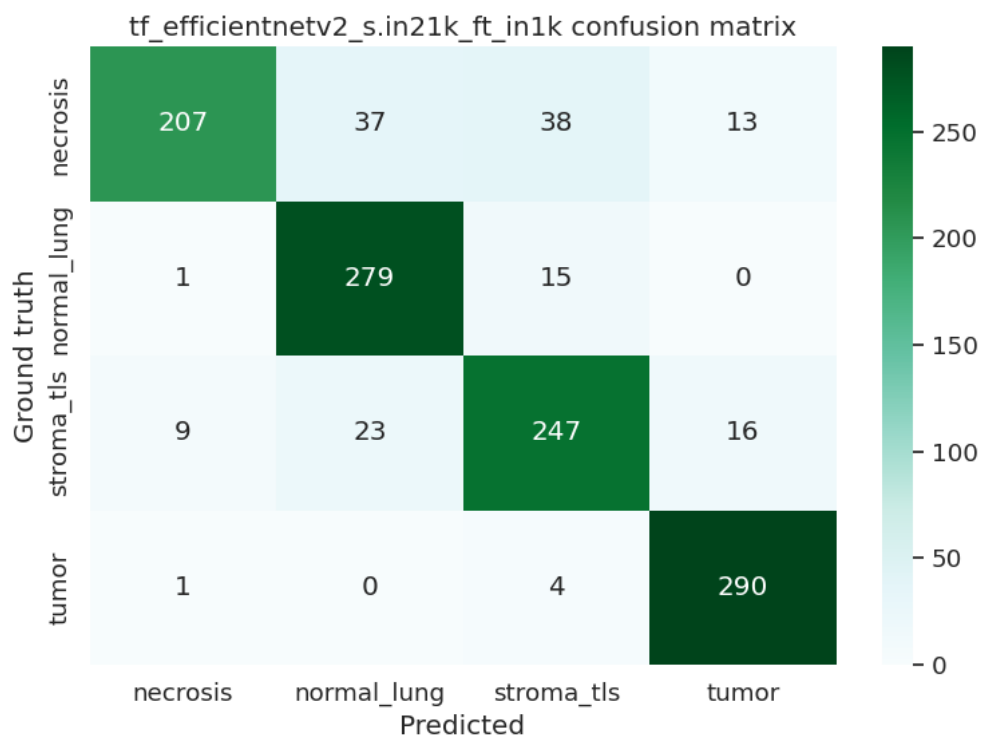


Figure A2.1 Confusion matrix of the classification model for the test subset

Patch ratio	c-index (average)	Standard deviation	Number of patches (average)
0.005	0.63214	0.0113	21
0.01	0.63904	0.0083	42
0.05	0.64851	0.0035	215
0.1	0.65090	0.0023	432
0.2	0.65144	0.0017	864
0.3	0.65177	0.0014	1297
0.4	0.65209	0.0010	1730
0.5	0.65190	0.0009	2163

Table A2.1 Analyzed patch ratios and corresponding c-index calculated using Monte-Carlo simulation and 100 iterations

A3. Supplementary Validation

	Overall cohort					Validation cohort					Training cohort				
	TILs score					TILs score					TILs score				
	Q1	Q2	Q3	Q4	<i>p</i>	Q1	Q2	Q3	Q4	<i>p</i>	Q1	Q2	Q3	Q4	<i>p</i>
Age															
<65	55	55	44	53	0.447	52	43	38	45	0.7	3	12	6	8	0.398
≥65	70	69	80	71		69	55	66	61		1	14	14	10	
Gender															
Female	37	35	44	44	0.474	36	31	37	40	0.58	1	4	7	4	0.439
Male	88	89	80	80		85	67	67	66		3	22	13	14	
Weightloss															
<10%	114	110	107	116	0.330	110	90	87	100	0.1	4	20	20	16	0.091
≥10%	11	14	16	8		11	8	16	6		0	6	0	2	
Smoking status															
Never smoked	5	4	1	7	0.159	5	2	0	6	0.16	0	2	1	1	0.298
Present smoker	71	77	85	83		70	63	71	69		1	14	14	14	
Previous smoker	49	43	38	34		46	33	33	31		3	10	5	3	
ECOG status															
Normal	62	74	75	83	0.092	60	64	63	69	0.14	2	10	12	14	0.119
Slightly reduced	49	41	42	37		48	29	35	33		1	12	7	4	
In bed <50%	14	9	7	4		13	5	6	4		1	4	1	0	
Histology															
LUSC	69	66	61	81	0.106	66	52	49	67	0.14	3	14	12	14	0.610
LUAD	55	57	60	41		54	46	52	37		1	11	8	4	
LULU	0	0	2	1		0	0	2	1		0	0	0	0	
LUAS	1	1	1	0		1	1	1	0		0	0	0	0	
NOS	0	0	0	1		0	0	0	1		0	0	0	0	
pStage															
IA	29	30	33	41	0.122	28	24	30	35	0.11	1	6	3	6	0.879

IB	20	18	28	12		19	13	23	11		1	5	5	1	
IIA	9	10	14	12		8	7	11	10		1	3	3	2	
IIB	29	29	25	36		29	21	19	31		0	8	6	5	
IIIA	34	31	18	20		33	27	15	16		1	4	3	4	
IIIB	4	6	6	3		4	6	6	3						
Differentiation															
Poor	52	48	56	50	0.794	51	39	47	42	0.95	1	9	9	8	0.624
Moderate	56	58	53	51		53	45	43	45		3	13	10	6	
Well	17	18	15	23		17	14	14	19		0	4	1	4	
Vascular invasion															
No	103	105	99	103	0.773	100	82	85	87	0.98	3	23	14	16	0.331
Yes	22	18	24	20		21	15	18	18		1	3	6	2	

Table A3.1 Quantized TILs score and its distribution over and correlation with clinicopathological variables

	All patients					Validation patients					Train patients				
	TILs_score_rnd_0.05					TILs_score_rnd_0.05					TILs_score_rnd_0.05				
	Q1	Q2	Q3	Q4	<i>p</i>	Q1	Q2	Q3	Q4	<i>p</i>	Q1	Q2	Q3	Q4	<i>p</i>
CD3															
[0,1e+03]	114	101	87	59	<0.001	110	82	71	53	<0.001	4	19	16	6	0.017
(1e+03,5e+03]	11	22	36	61		11	16	32	51		0	6	4	10	
CD4															
[0,550]	99	80	62	57	<0.001	96	66	51	53	<0.001	3	14	11	4	0.050
(550,5e+03]	25	41	60	67		24	31	51	53		1	10	9	14	
CD8															
[0,500]	82	59	56	35	<0.001	79	48	44	30	<0.001	3	11	12	5	0.144
(500,5e+03]	43	65	68	89		42	50	60	76		1	15	8	13	
CD20															
[0,400]	112	101	98	91	0.010	108	80	82	77	0.010	4	21	16	14	0.965
(400,5e+03]	12	22	26	33		12	17	22	29		0	5	4	4	

Table A3.2 Quantized TILs score and its distribution over and correlation with IHC based immune cell marker subsets

	Overall cohort					Validation cohort					Training cohort				
	N(%)	5 Year	Median	HR(95%CI)	p	N(%)	5 Year	Median	HR(95%CI)	p	N(%)	5 Year	Median	HR(95%CI)	p
CD8_posmm2_median															
Q1	127(26)	46	45	1	<0.001	111(26)	46	45	1	<0.001	16(24)	40	25	1	0.08
Q2	124(25)	53	98	0.81(0.53-1.22)		108(25)	52	73	0.87(0.56-1.35)		16(24)	61	NR	0.47(0.13-1.66)	
Q3	120(24)	70	235	0.49(0.33-0.74)		101(24)	66	NR	0.54(0.35-0.84)		19(28)	88	235	0.24(0.07-0.82)	
Q4	126(25)	71	NR	0.5(0.33-0.75)		109(25)	72	NR	0.45(0.3-0.69)		17(25)	62	84	0.73(0.2-2.58)	
TILs_score_rnd_0.05															
Q1	125(25)	39	37	1	<0.001	121(28)	39	37	1	<0.001	4(6)	33	30	1	0.12
Q2	124(25)	52	71	0.73(0.47-1.12)		98(23)	51	71	0.72(0.46-1.14)		26(38)	53	61	0.75(0.09-6.41)	
Q3	124(25)	69	NR	0.43(0.28-0.65)		104(24)	67	NR	0.46(0.3-0.72)		20(29)	78	NR	0.28(0.03-2.39)	
Q4	124(25)	78	235	0.3(0.2-0.45)		106(25)	79	NR	0.28(0.18-0.43)		18(26)	72	235	0.35(0.04-2.96)	

Table A3.3 Quantized CD8 TILs density and TILs score as predictors of disease-specific survival in non-small cell lung cancer patients

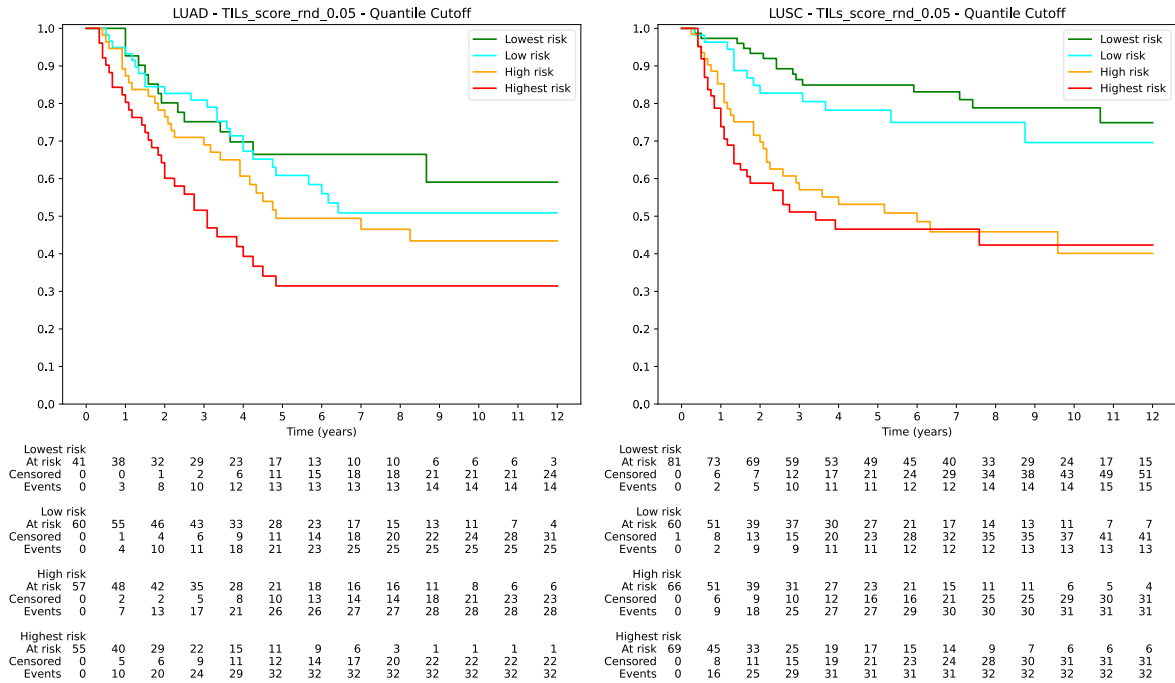


Figure A3.1 KM curves for TILs score using histology types for 497 patients

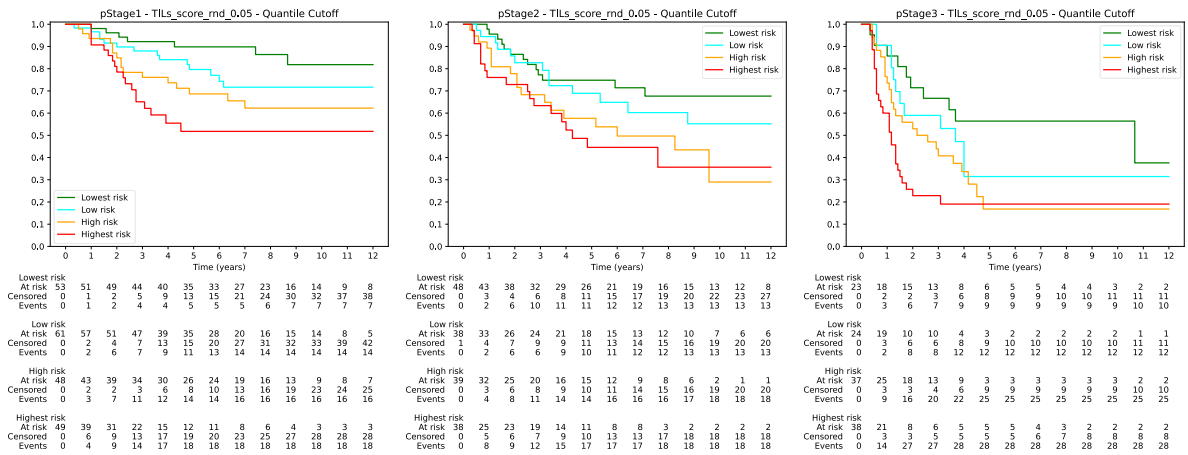


Figure A3.2 KM curves for TILs score using pStage information for 497 patients